On the possibilities of x-ray phase contrast microimaging by coherent high-energy synchrotron radiation

A. Snigirev and I. Snigireva
ESRF, B.P. 220, 38043 Grenoble Cedex, France

V. Kohn
Russian Research Centre, "Kurchatov Institute," 123182 Moscow, Russia

S. Kuznetsov and I. Schelokov
Institute of Microelectronics Technology RAS, 142432 Chernogolovka, Moscow region, Russia

(Received 26 April 1995; accepted for publication 5 September 1995)

Coherent properties of the x-ray beam delivered at the ESRF allow the observation of very weak perturbations of the wave front, resulting in the phase contrast. A straightforward experimental setup for phase contrast imaging is proposed and used to record holographic images from organic samples of 10–100 μm at energy 10–50 keV with the contrast up to 50%–100%. The theory of phase contrast imaging is considered and some theoretical estimations are made to reveal the performance of the proposed technique in terms of resolution, sensitivity, geometrical requirements, and energy range applicability. It is found that for carbon-based fibers a detectable size with 2% contrast is 0.1 μm for 10 keV and -1 μm for 100 keV. It is demonstrated that the fine interference structure of the image is very sensitive to the shape, density variation, and internal structure of the sample. Some prospects for the practical use and future development of the new coherent techniques such as phase contrast microscopy, microtomography, holography, and interferometry at high energies are also discussed. © *1995 American Institute of Physics.*

I. INTRODUCTION

X-ray imaging at high energies (>6 keV) such as contact radiography, projection microscopy, and tomography has been used for many years to nondestructively discern the features of the internal structure of the objects in material science, biology, and medicine. In so doing the main contrast formation is an absorption that makes some limitations for imaging of the light density materials and, what is more important the resolution of contact radiography and tomography is not better than 10–100 μm, depending on the applications. It turned out that for imaging at micrometer and submicrometer resolution there is no way to overcome these limits except phase contrast imaging. It is well known in optics that the phase contrast is realized in a phase contrast microscopy suggested by Zernike and Gabor (in-line) holography when interference between reference wave front and transmitted through the sample takes place. Both of these techniques, phase contrast x-ray microscopy[1,2] and holography,[3,4] are successfully progressing now in the soft x-ray region. For imaging in the hard x-rays to enhance the contrast and to be able to resolve phase variations across the beam, a high degree of coherence is needed. Because of this it was reasonable that the perfect crystal optics were involved such as a Bonse–Hart interferometer,[5,6] double-crystal, and even triple-crystal setup using Laue and Bragg geometry with asymmetrically cut crystals.[7–10]

In this article we would like to demonstrate that in the case of high spatial coherency of the beam provided by the third generation of the synchrotron radiation sources like ESRF—source size ~100 μm, quite large source-to-object distance ~50 m, and presence of the Si monochromator—it is possible to realize a phase contrast imaging directly from the sample in the transmission geometry. This idea is closely similar to in-line holography, where the radiation scattered by the sample interferes with a coherent incident monochromatic beam and this interference pattern is recorded with a high-resolution detector (film) located at a certain distance. Unlike the techniques,[7–10] in this setup an analyzer crystal is not necessary and even harmful; this is because first, the linear resolution of the crystal itself is limited by extinction depth, and second, the phase interference contrast will be diminished since a narrow angular acceptance of the crystal analyzer causes to cutting the angular spectrum of the diffracted pattern. We experimentally show that a well-collimated coherent beam at 10–50 keV allows to make visible very small and light density objects like organic fibers which do not absorb practically the incident radiation and only produce an inhomogeneous phase shift in the part of the wave front of the radiation. It should be noted that on the other hand this extreme and in some cases "superfluous" coherence leads to the undesirable impacts that impose special requirements on all elements to be installed in the beam path, such as, for example, beryllium windows.[11]

II. EXPERIMENT

In fact first phase contrast images of the light density materials were observed at the microdiffraction experiments with the Bragg–Fresnel lenses (BFLs).[12,13] These images were used to locate the small light density specimens: 10–100 μm organic fibers and 50 μm starch granules in the sub-μm x-ray beam generated by BFLs. The surprising thing was that almost transparent fibers produced images with a high contrast at 14 keV. At that moment it has been realized that this contrast had a phase nature but no complete understanding has been achieved. In this work we made a

 0034-6748/95/66(12)/5486/7/$6.00

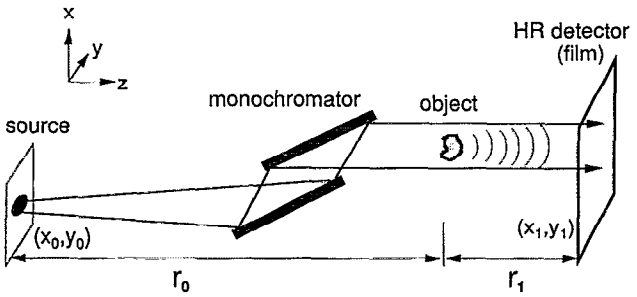

FIG. 1. Schematic display of the experimental setup, where r_0 is the distance from the source to the fiber (40 m) and r_1 is the distance from the fiber to the high-resolution film (from 20 to 200 cm).

systematic experimental study of imaging different fibers and other light density materials in different experimental conditions.

The experiment was done at the ESRF Optics beamline. The experimental setup is shown schematically in Fig. 1. The 10–50 keV radiation from bending magnet was selected by a Si(111) monochromator. Specimens were located 40 m from the source. The sample stage consists of a two-axis motor driven translation stage (Y,Z). the (Y,Z) stage was used for the adjustment of the sample to the beam. The x-ray images were recorded using Kodak high-resolution films and an x-ray high-resolution CCD camera from Photonic Science, which were placed at the distances r_1 from the sample position in the range 0–200 cm.

It is easy to show when a nearly parallel monochromatic x-ray beam impinges on the surface of a practically transparent light density specimen there will always be an apparent deviation from the rectilinear x-ray propagation—the segments of the wave front will be deflected due to refraction at a sloping sample-air interface. Further interpositioning of the deflected coherent rays will cause strong interference at a certain distance. Rough estimations for the energy range 10–50 keV show that the angle of deflection is about 10^{-5}–10^{-6} rad and 5–10 μm intersection of the beams may occur at the 1 m distance from the sample.

The experimentally obtained x-ray holograms of the 10 μm cellulose fiber at variable sample-to-film distances are shown in Fig. 2. The calculated intensity profiles across the fiber according the theory presented in next chapter are presented in Fig. 2 as well. Due to the phase contrast imaging the fibers are clearly discernible at distances beginning from a few centimeters. As viewed from Fig. 2(a) at a distance about 25 cm between fiber and film the two very strong intensity maxima corresponding to the fiber edges are observed. With the increasing the fiber–film distance the third not so strong intensity maximum appears appropriating to the central part of the fiber. Further increasing the fiber–film distance leads to the broadening of the intensity peaks and a decrease of the intensity maximums.

The x-ray holograms gathered from the 20 μm polypropylene fiber at different fiber–film distances (from 20 to 150 cm) and relative calculated intensity profiles across the fiber are demonstrated in Fig. 3. At shorter distances (less than 200 cm) a very fine interference pattern can be seen between two intensity maximums. At larger distances (more than 200

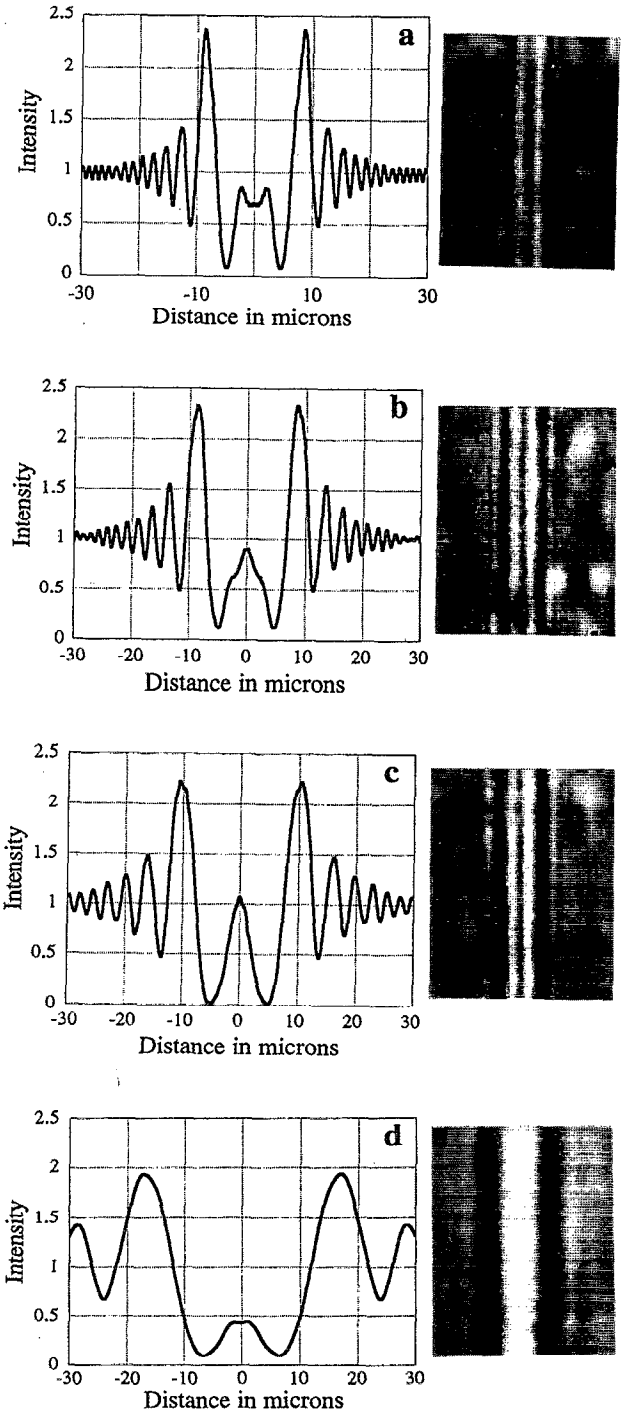

FIG. 2. Experimental x-ray holograms of the 10 μm cellulose fiber at different distances and relative theoretical intensity distribution (in arbitrary units) across the fiber: (a) 0.25 m, (b) 0.3 m, (c) 0.5 m, and (d) 2 m.

cm) for a 20 μm fiber the behavior of the intensity profile is similar to a 10 μm fiber, for example, the x-ray image of a 10 μm fiber at 50 cm looks the same as for a 20 μm fiber at 200 cm.

As a further demonstration of the proposed setup the phase contrast image of green paper used for alignment is shown in Fig. 4. On the image one can see the internal mesh structure of the paper. In Fig. 5 the phase contrast images of very thin slightly melted Al foil at (a) 25 cm and (b) 150 cm

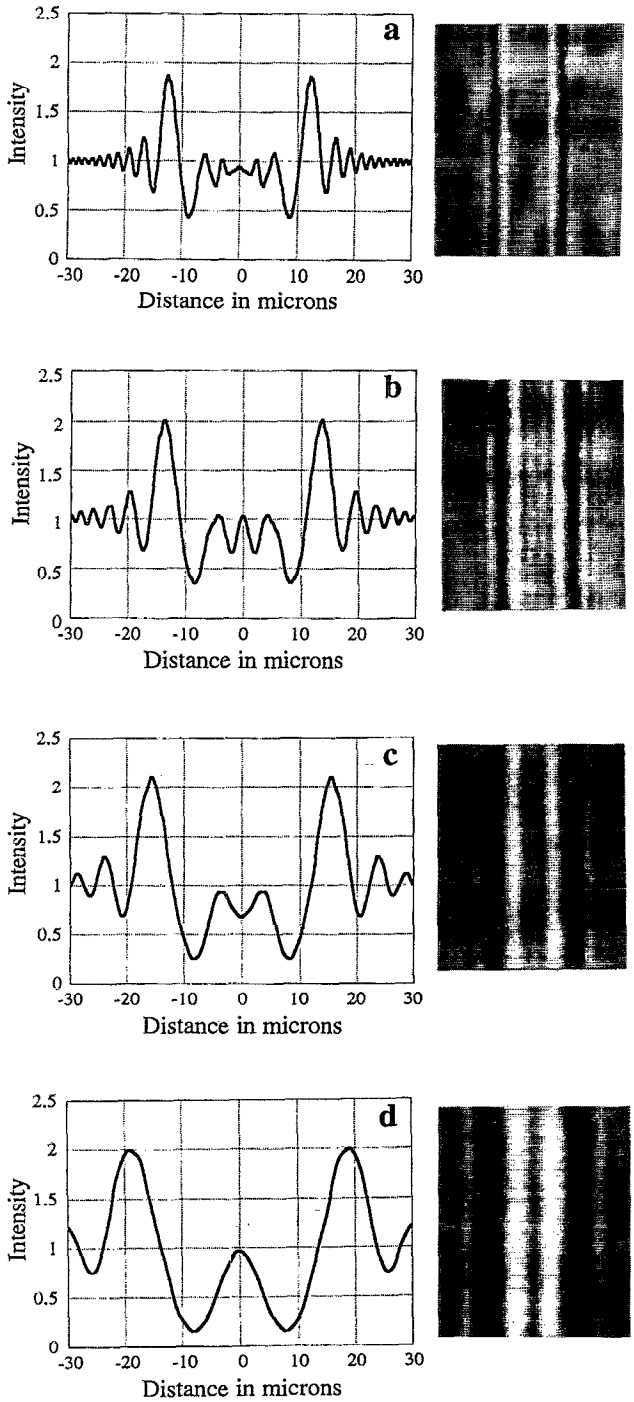

FIG. 3. Experimental x-ray holograms of the 20 μm polypropylene fiber at different distances and theoretical intensity distribution (in arbitrary units) across this fiber: (a) 0.25 m, (b) 0.5 m, (c) 1 m, and (d) 2 m.

distances are presented. With the distance the fine interference structure has a tendency to vanish.

As has already been intimated from the experimental images there are two main features: first strong black and white contrast on the fiber edges, that can be explained by the refraction-index difference, and second, the very fine interference pattern. The two intensity maximum might be useful for locating the fibers in the sub-μm x-ray beam and for diagnosing the surface defects and morphology of the fiber

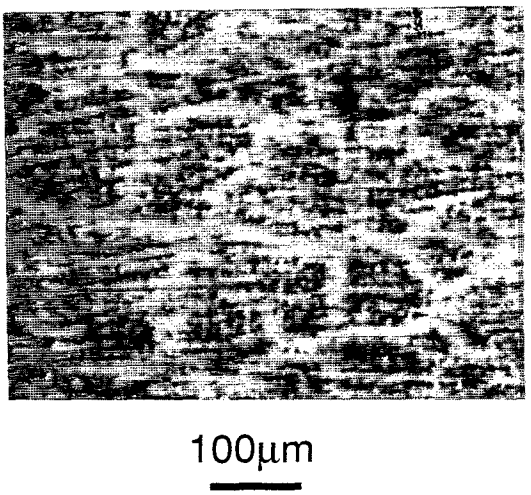

FIG. 4. Experimentally obtained x-ray phase contrast image of the green paper.

surface. One of the most promising applications for the fine interference pattern will be a determination of the internal fiber structure and fiber shape as well.

It is not trivial to describe the character of observed phase contrast on the basis of the qualitative reasoning. To gain greater insight into phase contrast formation the theoretical analysis and some estimations were done and they are presented in the next chapter.

III. THEORETICAL ANALYSIS OF PHASE CONTRAST FORMATION

The theory of the phase contrast microimaging is similar to the theory of laser optics in-line holography of small particles (see, for example, Ref. 14). However, owing to the fact that for hard x rays the wavelength is very short, the Fraunhofer or far-field approximation is not valid in general. Also we shall consider here the case of a spherical incident wave taking into account the source-to-object distance.

Let us consider the pure coherent radiation from a point source placed in the plane perpendicular to the z axis at the point x_0, y_0. According to Maxwell's equation, in the free space this radiation is the spherical wave and it can be written in the form

$$E_0(x_1,y_1)=\frac{1}{r}\exp\left[\frac{2\pi i}{\lambda}\left(r+\frac{(x_1-x_0)^2}{2r}+\frac{(y_1-y_0)^2}{2r}\right)\right], \quad (1)$$

where x_1, y_1 are the coordinates of the point in the 2D-detector plane, r is the distance between the source and the detector planes, λ is an x-ray wavelength. Here we suppose a small angle approximation which is valid when $r^2 \gg (x_1-x_0)^2+(y_1-y_0)^2$.

When the phase object (for example, fiber) is placed between the source plane and the recording plane, we have to take into account an additional phase shift of the field. It is convenient to consider a thin layer containing the fiber and having the plane boundaries. Inside the layer the wave field will have the slowly variable coefficient before a fast oscillating exponent function. Similar to the x-ray crystal optics

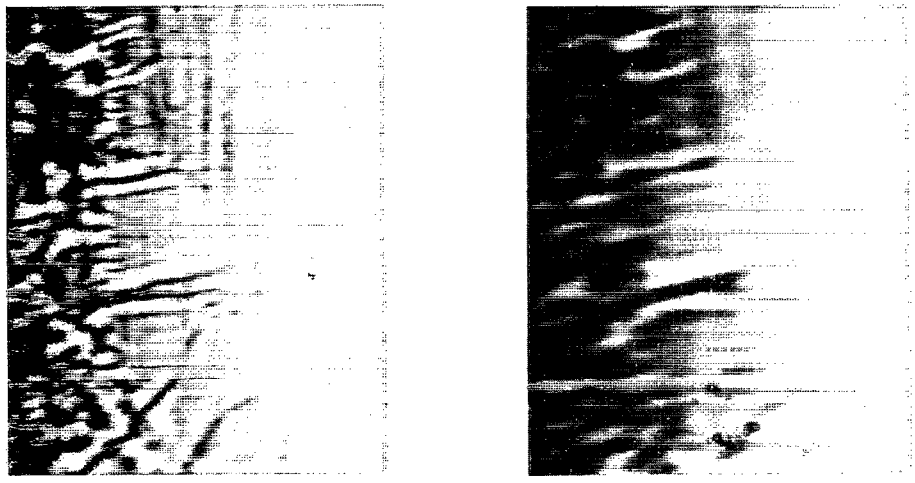

FIG. 5. X-ray phase contrast images of the slightly melted Al foil at distances (a) 25 cm and (b) 150 cm at 16 keV radiation.

theory,[15] in this case the truncated equation for a slowly variable coeffiient can be considered with only the derivative in the direction of the incident beam. As a result we surmised that the light density object simply delays an incident wave front by the amount proportional to the effective thickness of the sample at each point.

Let us consider the case when the change of phase front takes place only in an x direction and define it as a function $\varphi(x)$. This corresponds to the linear objects such as a fiber oriented along the y axis. By means of a standard Kirchhoff integral,[16] we can express the radiation field in the hologram plane in the next form

$$E(x_1,y_1)=\frac{1}{\sqrt{i\lambda r r_0 r_1}}\exp\left[\frac{2\pi i}{\lambda}\left(r+\frac{(y_1-y_0)^2}{2r}\right)\right]\times\int dx\,\exp\left[\frac{2\pi i}{\lambda}\left(\frac{(x-x_0)^2}{2r_0}+\frac{(x-x_1)^2}{2r_1}\right)\right]\exp[i\varphi(x)], \tag{2}$$

where r_0 and r_1 are the source-to-object and object-to-hologram distances (see Fig. 1). This formula allows the calcultion of the general case of an arbitrary phase object.

Let us consider the case when the object has a finite size, for example, in the range $-R<x<R$. To calculate the relative intensity distribution it is convenient to rewrite Eq. (2) as follows:

$$E(x_1,y_1)=E_0(x_1,y_1)[1+c(x_1)], \tag{3}$$

where the function directly responsible for the formation of the fiber image takes the form

$$c(x_1)=\sqrt{\frac{r}{i\lambda r_0 r_1}}\exp\left[\frac{2\pi i}{\lambda}\left(-\frac{(x_1-x_0)^2}{2r}\right)\right]\times\int_{-R}^{R}dx\,\exp\left[\frac{2\pi i}{\lambda}\left(\frac{(x-x_0)^2}{2r_0}+\frac{(x_1-x)^2}{2r_1}\right)\right]\times\{\exp[i\varphi(x)]-1\}. \tag{4}$$

Correspondingly the intensity normalized on the background value (without the fiber) is given by

$$I(x_1)=1+2\,\mathrm{Re}[c(x_1)]+|c(x_1)|^2. \tag{5}$$

If the source has significant size or the 2D detector has a finite resolution, we have to integrate the intensity over the source coordinates and average over the characteristic region of the detector resolution. Equations (4) and (5) were used in this work to simulate the images given by the fibers of different sizes at a different distances.

In the laser optics in-line holography of small particles[14] the square modulus term in Eq. (5) is usually omitted. It allows the use of a simple reconstruction technique. In this work we are not interested in the reconstruction of the image because it is not that simple for the phase object. Instead we would like to study the possibilities of the phase object imaging in the general case, where the contrast may reach 100% and a square modulus term is essential.

It is clear that the inhomogeneous intensity distribution arises on the hologram within the finite region which increases in size with increasing the distance r_1. In the case when $r_0 \gg r_1$ the size of the source and the distance r_0 are not so important. For the plane incident wave when $r=r_0=\infty$, we obtain a more simple expression

$$c(x_1)\approx\frac{1}{\sqrt{i\lambda r_1}}\int_{-R}^{R}dx\,\exp\left[\frac{2\pi i}{\lambda}((x_1-x)^2)2r_1\times\{\exp[i\varphi(x)]-1\}. \tag{6}$$

Let us consider this case in more detail. When r_1 is small enough, the exponent function which is really the propagator of the radiation from the object plane to the recording plane is a very fast oscillating function. We can estimate the integral by means of a stationary phase. This leads to the result as the propagator is replaced by a delta function and the phase modulation of the field is conserved and the imaging the phase object is absent.

To obtain the image at short distances from the object the latter must have some fragments which delay the phase with significant inhomogeneity as compared with the propagator. If a size of this region is d, then the effect discussed above arises at the distance $r_1 > d^2/\lambda$. It is a distance of extreme Fresnel diffraction. Actually, as it was shown by computer calculations, a small contrast arises at a shorter distance; it depends on the definition of the parameter d.

For example, a circular fiber has the following phase function

$$\varphi(x) = \frac{4\pi}{\lambda}\,\delta R\sqrt{1-\left(\frac{x}{R}\right)^2}, \tag{7}$$

where δ is the decrement of refraction. It has a negative value for x rays. The faster change of the phase takes place at the sides where d can be estimated as $0.1R$. This determines the shorter distance of fiber imaging $L_s = 0.01R^2/\lambda$. For example, for the fiber of $R = 5$ μm and the radiation of $E = 10$ keV we can evaluate the minimum distance as $L_s \approx 0.2$ cm. At this distance only small parts of the fiber can be seen. To obtain the distance where all parts of the fiber contribute to the contrast we have to take $d = R/2$. This determines the middle distance of imaging $L_m = R^2/4\lambda$, that is, the distance of Fresnel diffraction.[17] For the conditions discussed above we have $L_m \cong 5$ cm. Finally, $d = 2R$ determines the lower boundary of the large distances $L_l = 4R^2/\lambda$, where the phase of the propagator changes very slowly inside the integration region. It is the case of Fraunhofer diffraction where the far-field condition is valid.[14] In this region of distances r_1 the image has the definite unchanged form but the size of this image increases monotonously with r_1 while the contrast monotonously decreases. In the considering case $L_l = 80$ cm.

IV. DISCUSSION

It makes sense to consider some peculiarities of the proposed technique and give some estimations for the sensitivity and resolution. There is an interesting question of what is the minimum diameter of the light density fiber that can be imaged using the proposed method. Let us determine the contrast parameter C as a maximum different between positive and negative deviations of the intensity from the unit. One can make the following estimations for C in the Fresnel region $C = \alpha\,\varphi_0$, where α is a numerical coefficient which is close to unity and φ_0 is a maximum value of the phase delay. This estimation was obtained from the analysis of various computer simulations of the fiber images.

As it is known $\varphi_0 = 2\pi\delta h/\lambda$, where δ is the decrement of refraction and h is the maximum size of the fiber in the direction of the x-ray beam. On the other hand it is known

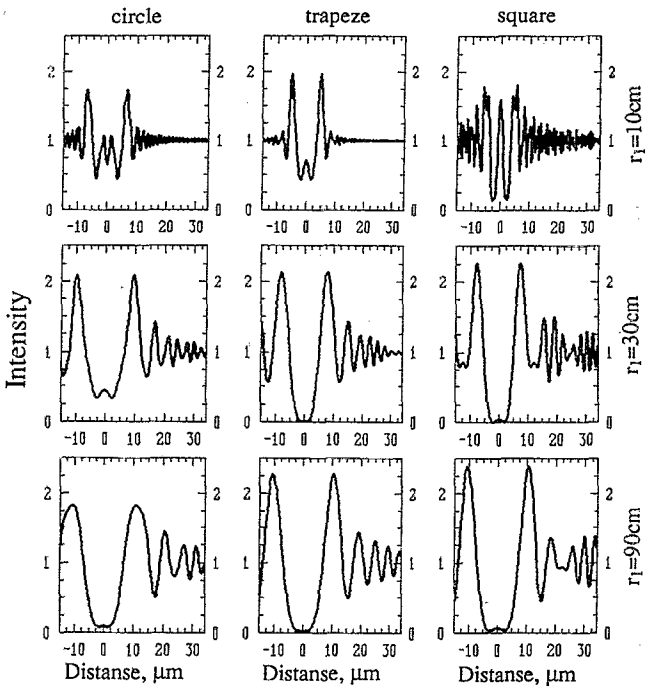

FIG. 6. Theoretical intensity distribution (in arbitrary units) across the 10 μm beryllium fiber various shapes: round, trapezium, and square at different distances: 10, 30, and 90 cm.

that δ depends on the wavelength value λ as $\delta = \gamma\lambda^2$. Taking this into account the following formula for the contrast parameter can be obtained

$$C = 2\pi\alpha\gamma\lambda h. \tag{8}$$

Considering the estimation for the contrast parameter (8) we can calculate the contrast of the 0.1-μm-thick carbon-based fiber with decrement of refraction $\delta = 4.7\times10^{-6}$. For $\alpha = 1$, $\lambda = 1.24\times10^{-10}$ m ($E = 10$ keV), $\gamma = 3.05\times10^{14}$, and $h = 0.1$ μm the contrast $C = 2\%$ can be obtained, which is experimentally detectable. Since the contrast behavior is linear with the wavelength of the x rays, one can predict the same values for a contrast of 2%–3% for a 1 μm fiber at 100 keV. As far as no magnifying optics were used in our experiment the resolution is limited by the resolution of the detector, that is, 1 μm for high-resolution x-ray film. One cannot forget to apply in the future a high-resolution photoresist like in soft x-ray holography.[3,4]

It should be noted that the real image pattern, as it follows from the theoretical analysis, depends on the shape of the fiber. In Fig. 6 are displayed the calculated intensity profiles for 10 μm fibers of different shapes: round, trapezium, and square. In this case fiber with a decrement of refraction $\delta = 5\times10^{-6}$ was used which corresponds to beryllium at 10 keV. At short distances profiles look totally dissimilar; in addition to two maxima corresponding to the edges of the fiber one can find a minimum of intensity for the round fiber, a small maximum for the trapezium fiber, and a high maximum for the square fiber corresponding to the central part of the fiber. At large distances fiber-to-detector profiles become similar in appearance, and at distances more that 100 cm profiles look very akin.

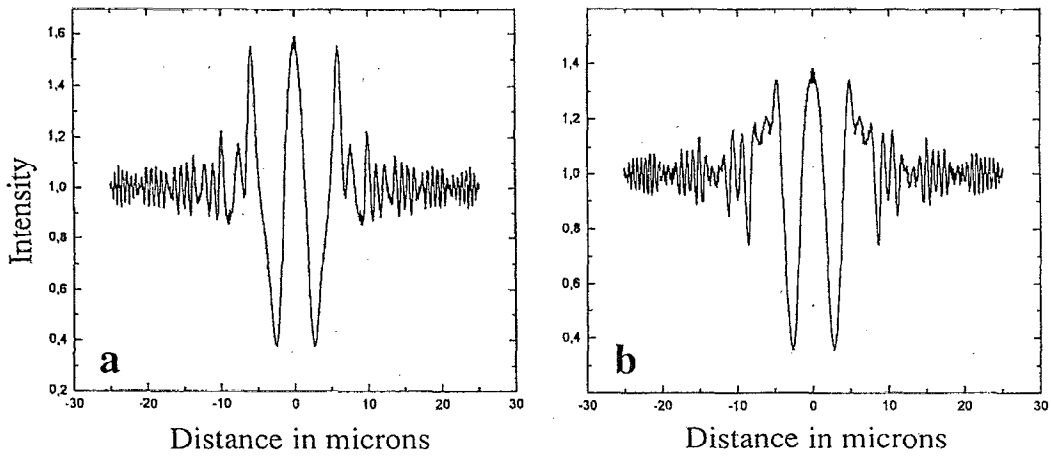

FIG. 7. Calculated intensity distribution (in arbitrary units) across the capillaries with 10 μm external diameter and 3 μm (a) and 2μm (b) internal diameter at distance 20 cm.

The diffraction pattern is very sensitive to the variations of the refraction index inside the sample, especially if this variation is regular and can be used for diagnostics of, for example, glass capillaries. As a proof of high sensitivity of the proposed method the calculated intensity distribution across the capillaries with 10 μm external diameter and (a) 3 μm and (b) 2 μm internal diameter are shown in Fig. 7.

We would like to mention that the time coherence provided by a silicon monochromator is vastly superior to what is needed for this technique. However monochromators with wider bandpass such as, for example, multilayers, will tend to deterioration of the spatial coherence because of their imperfections.

V. APPLICATIONS

There is no doubt that demonstrated phase contrast sensitivity has a practical applicability. Moreover, it drastically improves the efficiency and the resolution of the existing x-ray diagnostic techniques. The availability of the strong interference structure related to the edges of the sample allows one to locate micrometer objects (fibers and single granules 1–10 μm size) in the x-ray microbeam with an accuracy of about 1 μm (Refs. 12 and 13) with a high-resolution film. It is clear that the alignment can be improved using the intensity mapping by scanning a 5–10 μm pinhole coupled with the detector across the fiber image at the proper distance from the specimen. Certainly the high coherence of the x-ray beam must be taken into consideration for x-ray topography when the film is placed at some distance from the sample. Moreover invoking the phase contrast can provide additional information about an imperfection of the internal structure as well as about a topology of the surface.

Basically from the experimental results presented above and the theoretical calculations, the advancement of coherent optics techniques such as phase contrast microscopy, phase contrast tomography, interferometry, and holography is apparent.

A. Holography and interferometry

As mentioned above, the experimental setup shown in Fig. 1 is conceptually identical with the approach used in the Gabor in-line holography where the detector records the interference between roughly spherical waves scattered by the sample with plane reference waves coming directly from the illuminating source.[3,4,14] The interference pattern contains full information about the size, shape, and other features of the sample. In principle the holograms recorded in high-resolution film or resist can be reconstructed by means of a numerical technique. Fourier holography[18] in high-energy domain is feasible as well on the basis of Bragg–Fresnel optics (BFO). The fine interference pattern can be used for the determination of high accuracy optical density and refraction index.

B. Phase contrast microscopy

Phase contrast x-ray microscopy at high energy based on BFO has considerable promise while we are dealing with the very coherent parallel illumination.[19–21] In put forward phase contrast microscopy the depth of the image field is almost infinite, as in laser microscopy, and therefore the method of "defocusing" will only reveal the phase contrast and will not cause the resolution to decrease.

C. Phase contrast microtomography

X-ray transmission computed tomography is based on getting cross-sectioned images as the absorbing density distribution. From this it is clear that this technique has some limitations for studying light density materials, especially with submicrometer resolution. Considering small divergence and coherent properties of the beam, the evident benefits might be achieved in developing phase contrast tomography. For phase contrast tomography with parallel illumination the resolution is determined by the resolution of the detector, that is, 5–10 μm for high-resolution x-ray cameras and 1 μm for high-resolution films at the moment. Using additional optics such as a Bragg–Fresnel lens installed after the object should lead to 0.1 μm resolution at 2% con-

trast detectability.[19–21] An experiment on phase contrast microtomography has been done and the manuscript is under preparation.

It should be noted at that the planning medical beamlines with the use of the perfect crystal monochromator the conditions to observe phase contrast are automatically fulfilled. Therefore the phase contrast mechanism has to be taken into account under registration and interpretation of the images. Moreover, the deliberate use of phase contrast imaging should significantly reduce the radiation dose.

High coherency of the beam provided by third generation of the synchrotron radiation allows phase contrast imaging in the very simple experimental setup. It was demonstrated that phase contrast images from light density materials, 10–20 μm sizes, are easily seen. According to the theoretical estimations the 0.1 μm light density carbon-based fiber can be visualized at 10 keV energy and a contrast of about 2% can be achieved. Specimen size and thickness can have large ranges depending on the applications. It was shown that the fine interference structure of the image is very sensitive to the shape, optical density, and internal inhomogeneity of the sample. Experimental images and theoretical calculations evidently show that the advancement phase contrast imaging techniques like microscopy, microtomography, holography, and interferometry are feasible and future perspectives for these new coherent techniques are described.

ACKNOWLEDGMENTS

We gratefully acknowledge A. Freund, and U. Lienert for his help and providing the beam time at the Optics beamline at the ESRF. Our thanks also go to J-M. Rigal and R. Hustache for their help in performing the experiments at the beamline.

[1] G. Schmahl, P. Gutmann, G. Schneider, B. Niemann, C. David. T. Wilhein, J. Thieme, and D. Rudolph, in *X-Ray Microscopy IY*, edited by V. V. Aristov and A. I. Erko (Bogorodski Pechatnik, Chernogolovka, Moscow region, 1994), pp. 196–206.
[2] D. Rudolph. G. Schmahl, and B. Niemann, in *Modern Microscopes*, edited by P. J. Duke and A. G. Michette (Plenum, New York, 1990), pp. 59–67.
[3] C. Jacobsen, M. R. Howells, J. Kirz, and S. Rohman, J. Opt. Soc. Am. A **7**, 1847 (1990).
[4] M. R. Howells, C. J. Jacobsen, and S. Lindaas, in *X-Ray Microscopy IY*, edited by V. V. Aristov and A. I. Erko (Bogorodski Pechatnik, Chernogolovka, Moscow region, 1994), pp. 196–206.
[5] U. Bonse and M. Hart, Appl. Phys. Lett. **6**, 155 (1965).
[6] A. Momose, T. Takeda, and Y. Itai, Rev. Sci. Instrum. **66**, 1434 (1995).
[7] E. A. Beliaevskaya, V. N. Ingal, and P. V. Petrashen, Proc. of 2nd European Symposium "X-Ray Topography and High Resolution Diffraction," Berlin, Germany, September 1994 (1994), p. 44.
[8] V. N. Ingal and E. A. Beliaevskaya, Proc. of 2nd European Symposium "X-Ray Topography and High Resolution Diffraction," Berlin, Germany, September 1994 (1994), p. 117.
[9] A. A. Manushkin, N. L. Mitrofanov, K. M. Podurets, V. A. Somenkov, and S. S. Shilstein, Proc. of 2nd European Symposium "X-Ray Topography and High Resolution Diffraction," Berlin, Germany, September 1994 (1994), p. 147.
[10] T. J. Davis, D. Gao, T. E. Gureyev, A. W. Stevenson, and S. W. Wilkins, Nature **373**, 595 (1995).
[11] A. Snigirev, I. Snigireva, V. Kohn, and S. Kuznetsov, Nucl. Instrum. Methods (to be published).
[12] A. Snigirev, I. Snigireva, C. Riekel, A. Miller, L. Wess, and T. Wess, J. Phys. IY **3**, 443 (1993).
[13] H. Chanzy, C. Riekel, I. Snigireva, and A. Snigirev, in *X-Ray Microscopy IY*, edited by V. V. Aristov and A. I. Erko (Bogorodski Pechatnik, Chernogolovka, Russia, 1994), pp. 273–275.
[14] G. A. Tyler and B. J. Thomson, Opt. Acta **23**, 685 (1976).
[15] Z. G. Pinsker, *Dynamical Scattering of X-Rays in Crystals* (Springer, Heidelberg, 1984).
[16] J. Cowley, *Diffraction Physics* (North-Holland, Amsterdam, 1975).
[17] J. W. Goodman, *Fourier Optics* (McGraw–Hill, New York, 1968).
[18] I. McNulty, J. Kirz, C. Jacobsen, E. H. Anderson, M. R. Howells, and D. P. Kern, Science **256**, 1009 (1992).
[19] A. Snigirev, Rev. Sci. Instrum. **66**, 2053 (1995).
[20] A. Snigirev, ESRF Newsletter No. 22, 20 (1994).
[21] A. Snigirev, I. Snigireva, P. Bosecke, and S. Lequien Opt. Commun. (to be published).